J. Fluid Mech. (1982), *vol.* 114, *pp.* 283–298
Printed in Great Britain

Analytic structure of vortex sheet dynamics. Part 1. Kelvin–Helmholtz instability

By DANIEL I. MEIRON, GREGORY R. BAKER AND STEVEN A. ORSZAG

Massachusetts Institute of Technology, Department of Mathematics, Cambridge, MA 02139

(Received 5 January 1981 and in revised form 28 May 1981)

The instability of an initially flat vortex sheet to a sinusoidal perturbation of the vorticity is studied by means of high-order Taylor series in time t. All finite-amplitude corrections are retained at each order in t. Our analysis indicates that the sheet develops a curvature singularity at $t = t_c < \infty$. The variation of t_c with the amplitude a of the perturbation vorticity is in good agreement with the asymptotic results of Moore. When a is $O(1)$, the Fourier coefficient of order n decays slightly faster than predicted by Moore. Extensions of the present prototype of Kelvin–Helmholtz instability to other layered flows, such as Rayleigh–Taylor instability, are indicated.

1. Introduction

It is well known that, in the absence of gravity or surface tension, tangential shear at a sharp interface is always destabilizing. For the classical Kelvin–Helmholtz instability, the linearized evolution of a normal mode with amplitude $A(k,t)$ and wavenumber k is given by

$$\frac{d^2A(k,t)}{dt^2} = \sigma^2 A(k,t),$$

where

$$\sigma(k) = \left(\frac{\rho\rho' k^2}{(\rho+\rho')^2}|u-u'|\right)^{\frac{1}{2}},$$

u and u' are the unperturbed velocities on either side of the interface and ρ and ρ' are the corresponding densities (see figure 1).

The disturbance grows at a rate $\sigma(k)$ which is directly proportional to the wavenumber k. As a result, an initial condition which is analytic in a finite strip (as reflected in the exponential decay of its Fourier coefficients with increasing wavenumber) will lose its analyticity after a finite time. At this critical time, the normal modes decay only as some algebraic power of the wavenumber and the interface develops a singularity.

The nonlinear dynamics of the interface can be expressed in terms of the dynamics of a vortex sheet. If $\rho = \rho'$ and $u = -u'$ then the interface,

$$z(e,t) = x(e,t) + iy(e,t),$$

satisfies the Birkhoff (1962) equation

$$\frac{\partial z^*(e,t)}{\partial t} = \frac{1}{2\pi i} P\int_{-\infty}^{\infty} \frac{\gamma(e',t)}{z(e,t)-z(e',t)}\,de'. \tag{1.1}$$

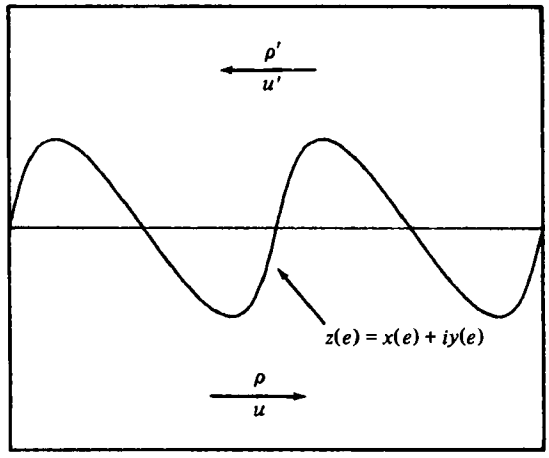

FIGURE 1. Flow geometry for the Kelvin–Helmholtz instability.

For convenience we refer to γ as the vortex sheet strength, although the true strength of the sheet is $\gamma(e,t)/(ds/de)$, where

$$\frac{ds}{de} = \left(\left(\frac{dx}{de}\right)^2 + \left(\frac{dy}{de}\right)^2\right)^{\frac{1}{2}}.$$

Also, the sheet strength $\gamma(e,t)$ is invariant along particle paths:

$$\frac{\partial \gamma(e,t)}{\partial t} = 0. \tag{1.2}$$

If the initial disturbances $z(e,0)$ and $\gamma(e,0)$ are periodic in the Lagrangian marker variable e, then the resulting sheet roll-up is also periodic in e. Thus, the interface z satisfies a periodic form of the Birkhoff equation, namely,

$$\frac{\partial z^*(e,t)}{\partial t} = \frac{1}{4\pi i} P \int_0^{2\pi} \cot \tfrac{1}{2}(z(e,t) - z(e',t))\, \gamma(e',t)\, de', \tag{1.3}$$

where the periodicity interval is $0 \leqslant e \leqslant 2\pi$.

It may be thought that nonlinear interactions restore the 'well-posedness' of the roll-up problem. Indeed, Sulem *et al.* (1982) have shown that an initially analytic interface remains so at least for a finite time. However, fully nonlinear numerical studies of Kelvin–Helmholtz instability using variants of the point vortex method give results that are unreliable (Van de Vooren 1965). As the number of vortex markers is increased chaotic vortex motion sets in at progressively earlier times. This evidence has led Birkhoff (1962) and Saffman & Baker (1979) to speculate that the solution of the nonlinear problem develops a singularity after a finite time. Such a singularity would not be inconsistent with the rigorous results of Sulem *et al.*

Recent numerical and analytical work by Damms (1978, unpublished), Moore (1979), respectively, give evidence that a weak singularity of the sheet does form after a finite time. They consider the problem in which

$$z(e,0) = e + \epsilon \sin e, \quad \gamma(e,0) = 1. \tag{1.4}$$

Then, the interface has the Fourier representation

$$z(e,t) = e + \sum_{m=-\infty}^{\infty} A_m(t) \exp(ime), \tag{1.5}$$

with $A_m = -A_{-m}$. Substituting the series (1.5) into (1.1) gives an infinite system of first-order differential equations for $A_m(t)$. Each equation has an infinite number of terms due to the complicated nonlinearity of the Birkhoff equation (1.1). Moore's asymptotic analysis takes into account the leading finite-amplitude corrections to linear theory. Each Fourier coefficient $A_m(t)$ is expanded in the form

$$A_m(t) = \epsilon^{|m|} A_{m0}(t) + \epsilon^{|m+2|} A_{m2}(t) + \epsilon^{|m+4|} A_{m4}(t) + \dots \tag{1.6}$$

and the subsystem of differential equations for A_{m0} is studied in detail. At a critical time $t_c(\epsilon)$ given to first order by

$$1 + \tfrac{1}{2} t_c + \ln t_c = \ln(4/\epsilon), \tag{1.7}$$

the coefficients A_{m0} decay like $m^{-\frac{1}{2}}$, indicating that z is no longer analytic in e. Damms (unpublished) has integrated numerically a truncated version of the evolution equations for the coefficients $A_m(t)$ and found good agreement with the asymptotics obtained at lowest order for small ϵ.

In the present work a prototype of the Kelvin–Helmholtz instability is proposed and examined. For our prototype problem, the sheet is initially flat but is set into motion impulsively by a sinusoidal disturbance of $\gamma(e)$:

$$z(e, t=0) = e, \quad \gamma(e, t=0) = 1 + a\cos e. \tag{1.8}$$

In § 2 it is shown that the asymptotic behaviour of the leading nonlinear corrections to the modal amplitudes is very similar to that found by Moore for initial condition (1.4). In § 3 the effects of the higher-order finite-amplitude corrections are examined by representing the solution as a Taylor series in time. The prototype initial condition (1.8) has the property that the Taylor series coefficient of $z(e,t)$ at any order $O(t^n)$ may be written as a finite Fourier series in e with n modes. The amplitudes of the modes are computed exactly using a spectral method. As a result of the simple structure of the series all finite-amplitude effects are incorporated at each order in time. Similar prototypical systems have been used to study the analytic structure of the Euler equations by Morf, Orszag & Frisch (1980). The singularity structure of the series is deduced using Padé approximants and the ratio method in § 4.

2. Moore's asymptotic analysis

We follow Moore in deriving the modal evolution equations for the prototype problem (1.1), (1.2) with initial condition (1.8). The substitution $e' = e + u$ in (1.1) gives

$$\frac{\partial z^*(e,t)}{\partial t} = \frac{1}{2\pi i} P \int_{-\infty}^{\infty} \frac{\gamma(e+u)\,du}{z(e,t) - z(e+u,t)},$$

where

$$z(e,t) - z(e+u,t) = -u + \sum_{m=-\infty}^{\infty} A_m(t) \exp(ime)\,[1 - \exp(imu)] = -u + s(u,e). \tag{2.1}$$

Substituting (2.1) into (1.1) gives

$$\sum_{m=-\infty}^{\infty} \frac{dA^*_m}{dt} \exp(ime) = -\frac{1}{2\pi i} P\int_{-\infty}^{\infty} \frac{du}{u}[1+\tfrac{1}{2}a\exp(i(e+u))+\tfrac{1}{2}a\exp(-i(e+u))] \times\left[1+\frac{s}{u}+\frac{s^2}{u^2}+\ldots\right].$$

Equating coefficients of $\exp(ime)$ gives the modal evolution equations

$$\begin{aligned}\frac{dA^*_m}{dt} = \frac{i}{2}\Big[&A_m I(m)+\frac{a}{2}A_{m-1}J(m)+\frac{a}{2}A_{m+1}K(m)\\ &+\ldots+\sum_{r_1+r_2+\ldots+r_k=m} A_{r_1}A_{r_2}\ldots A_{r_k}I(r_1,r_2,\ldots,r_k)\\ &+\frac{a}{2}\sum_{r_1+r_2+\ldots+r_k=m-1} A_r A_{r_2}\ldots A_{r_k}J(r_1,\ldots,r_k)\\ &+\frac{a}{2}\sum_{r_1+r_2+\ldots+r_k=m+1} A_{r_1},\ldots,A_{r_k}K(r_1,\ldots,r_k)\Big].\end{aligned} \tag{2.2}$$

The interaction coefficients I, J, K are defined by the integrals

$$\left.\begin{aligned} I(r_1,\ldots,r_k) &= P\int_{-\infty}^{\infty}(1-\exp(ir_1u))\ldots(1-\exp(ir_ku))\,u^{-(k+1)}du,\\ J(r_1,\ldots,r_k) &= P\int_{-\infty}^{\infty}\exp(iu)(1-\exp(ir_1u))\ldots(1-\exp(ir_ku))\,u^{-(k+1)}du,\\ K(r_1,\ldots,r_k) &= P\int_{-\infty}^{\infty}\exp(-iu)(1-\exp(ir_1u))\ldots(1-\exp(ir_ku))\,u^{-(k+1)}du.\end{aligned}\right\} \tag{2.3}$$

The sums in (2.2) range over all positive and negative integers so that each term has an infinite number of contributions. By introducing the ordering $A_m = O(a^{|m|})$ and its associated expansion

$$A_m = A_{m0}a^{|m|}+A_{m2}a^{|m+2|}+\ldots,$$

the system (2.2) reduces to subsystems for A_{m0}, A_{m2}, etc. The subsystem for A_{m0} is especially simple in that only positive values of the indices $r_1, r_2, \ldots, r_k$ occur. The sums involving the integral K are of higher order than $O(a^{|m|})$ and so only contribute to the higher-order subsystems. As the indices $r_1, r_2, \ldots, r_k$ are all positive the integrals I and J may be evaluated by residues

$$I(r_1,r_2,\ldots,r_k) = J(r_1,r_2,\ldots,r_k) = \pi(-i)^{k-1}r_1r_2\ldots r_k. \tag{2.4}$$

The equations for A_{m0} are, noting that $A_{-m}(t) = -A_m(t)$,

$$\begin{aligned}\frac{dA^*_{10}}{dt} &= \tfrac{1}{2}[(-i)A_{10}+\tfrac{1}{2}],\\ \frac{dA^*_{m0}}{dt} &= \tfrac{1}{2}[A_{m0}(-i)m+\tfrac{1}{2}A_{m-1,0}(-i)(m-1)\\ &\quad+\sum_{r_1+r_2=m}A_{r_10}A_{r_20}(-i)^2r_1r_2+\tfrac{1}{2}\sum_{r_1+r_2=m-1}A_{r_10}A_{r_20}(-i)^2r_1r_2\\ &\quad+\ldots+\sum_{r_1+r_2+\ldots+r_k=m}A_{r_10}A_{r_20}\ldots A_{r_k0}(-i)^kr_1r_2\ldots r_k\\ &\quad+\tfrac{1}{2}\sum_{r_1+r_2+\ldots+r_k=m-1}A_{r_10}A_{r_20}\ldots A_{r_k0}(-i)^kr_1r_2\ldots r_k],\end{aligned} \tag{2.5}$$

with the homogeneous initial condition

$$A_{m0}(t=0)=0. \tag{2.6}$$

The inhomogeneous term in the equation for A_{10} reflects the initial condition (1.8). As the equation for A_{m0} is linear with an inhomogeneous term involving only those coefficients A_{j0} for which $1<j\leqslant m-1$, the system (2.5) may be solved recursively. The solutions for A_{10}, A_{20}, and A_{30} are

$$\begin{aligned}
A_{10}(t) &= \tfrac{1}{2}\sinh\tfrac{1}{2}t+\tfrac{1}{2}i(\cosh\tfrac{1}{2}t-1),\\
A_{20}(t) &= [\tfrac{1}{16}t\cosh t-\tfrac{3}{16}\sinh t+\tfrac{1}{4}\sinh\tfrac{1}{2}t)]\\
&\quad +i[\tfrac{1}{16}t\sinh t-\tfrac{1}{8}\cosh t+\tfrac{1}{4}\cosh\tfrac{1}{2}t-\tfrac{1}{8}],\\
A_{30}(t) &= [\tfrac{1}{64}t^2\sinh\tfrac{3}{2}t-\tfrac{7}{96}t\cosh\tfrac{3}{2}t+\tfrac{119}{1152}\sinh\tfrac{3}{2}t\\
&\quad +\tfrac{1}{16}t\cosh t-\tfrac{3}{16}\sinh t-\tfrac{1}{64}t\cosh\tfrac{1}{2}t+\tfrac{15}{128}\sinh\tfrac{1}{2}t]\\
&\quad +i\,[\tfrac{1}{64}t^2\cosh\tfrac{3}{2}t-\tfrac{5}{96}t\sinh\tfrac{3}{2}t+\tfrac{7}{128}\cosh\tfrac{3}{2}t\\
&\quad +\tfrac{1}{16}t\sinh t-\tfrac{1}{8}\cosh t-\tfrac{3}{64}t\sinh\tfrac{1}{2}t+\tfrac{25}{128}\cosh\tfrac{1}{2}t-\tfrac{1}{8}].
\end{aligned} \tag{2.7}$$

From these first three solutions it is clear that

$$A_{m0}\simeq\exp(\tfrac{1}{2}mt)\,[\lambda_m^{(0)}t^{m-1}+\lambda_m^{(1)}t^{m-2}+\ldots]+O(\exp(\tfrac{1}{2}(m-1)t)).$$

The terms in the subsystem for A_{m0} arising from the condition $\Sigma_k r_k=m-1$ are $O(\exp(\frac{1}{2}(m-1)t))$. The dominant balance therefore involves only those terms which occur in the corresponding system for the initial condition studied by Moore (1979). The leading-order asymptotic behaviour of the two systems is essentially identical.

The result of Moore's analysis is that

$$a^mA_{m0}(t)\simeq C(t)\,m^{-\frac{5}{2}}\exp[m(1+\tfrac{1}{2}t+\ln(\tfrac{1}{4}at))], \tag{2.8}$$

where β is a normalization factor dependent only on t. At a critical time t_c defined by

$$1+\tfrac{1}{2}t_c+\ln t_c=\ln(4/a), \tag{2.9}$$

the coefficients decay algebraically rather than exponentially with increasing m. The approximation (2.8) is valid for $1\ll m\ll t\leqslant t_c$. A detailed discussion of the importance of the higher-order corrections and an improved estimate of the critical time may also be found in Moore's paper.

We have integrated numerically the system (2.5) for A_m. The results for $a=0{\cdot}0005$ are plotted in figure 2. The quantity $B_m=\ln|A_m(t)|$ is plotted *vs.* $\ln m$ for $1\leqslant m\leqslant 15$ at various times. At time $t=11{\cdot}30$, the results for B_m lie on a straight line whose slope is about $-2{\cdot}51$. The critical time predicted by (2.9) is $11{\cdot}15$, in good agreement with the computed value.

3. Taylor series expansion

In this section, the analytic structure of the prototype of Kelvin–Helmholtz instability evolving from the initial conditions (1.8) will be examined using Taylor series in time t. The interface $z(e,t)$ is expansible as

$$z(e,t)=e+\sum_{n=1}^{\infty}t^nZ_n(e). \tag{3.1}$$

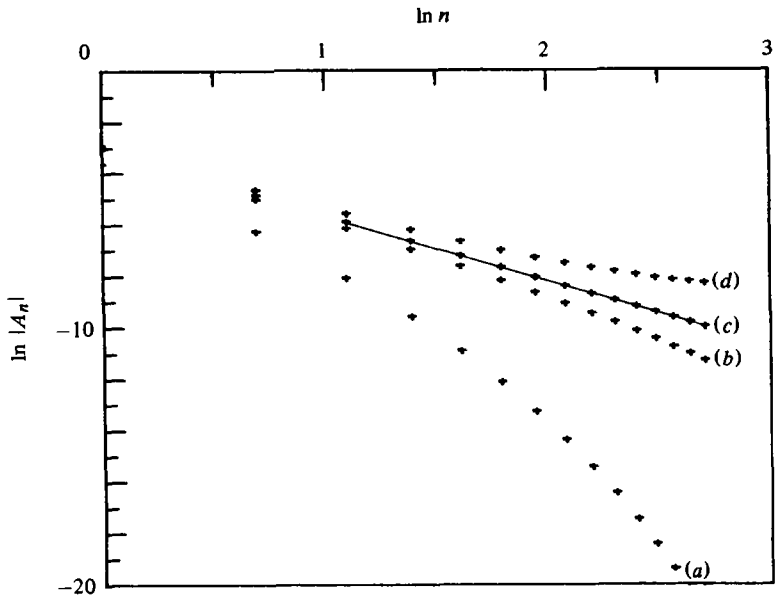

FIGURE 2. A plot of $\ln |A_n|$ *vs.* $\ln n$ showing the behaviour of the spectrum for the system of equations (2.2) at times (*a*) $t = 10{\cdot}04$, (*b*) $t = 11{\cdot}15$, (*c*) $t = 11{\cdot}30$, (*d*) $t = 11{\cdot}48$. The straight line fit at the singularity time $t = 11{\cdot}30$ gives a slope $\beta \simeq -2{\cdot}51$.

At $t = 0$, the interface is flat and $\gamma(e) = 1 + a\cos e$ so the Birkhoff equation gives

$$\frac{\partial z^*(e, t=0)}{\partial t} = \frac{1}{4\pi i} P\int_0^{2\pi} (1 + a\cos e')\cot \tfrac{1}{2}(e - e')\, de', \tag{3.2}$$

which is a periodic Hilbert transform in e. The integral is easily evaluated, giving

$$Z_1(e) = \frac{\partial z(e, t=0)}{\partial t} = \tfrac{1}{2} i a \sin e. \tag{3.3}$$

In order to obtain recursion relations for $Z_n(e)$ $(n > 1)$, the Birkhoff equation is regularized by adding and subtracting a known principal-value integral. Since

$$P\int_0^{2\pi} \cot \tfrac{1}{2}(z(e) - z(e'))\frac{dz(e')}{de'} de' = 0,$$

Birkhoff's equation may be rewritten as

$$\frac{\partial z^*(e)}{\partial t} = \frac{1}{4\pi i}\int_0^{2\pi} \left[\gamma(e') - \gamma(e)\frac{dz(e')/de'}{dz(e)/de}\right] \cot \tfrac{1}{2}(z(e) - z(e'))\, de'. \tag{3.4}$$

The first-order contribution (3.3) is a finite Fourier series. This result holds for the higher-order terms in the sense that

$$Z_n(e) = \sum_{m=0}^{n} Z_{nm} \sin me, \tag{3.5}$$

as will be shown below. For our prototype, it is possible to compute not only A_{m0} as simple power series in t, but also their higher-order corrections A_{mp} $(p \geqslant 2)$ as well as the exact-Taylor-series coefficients $Z_n(e)$. It should be noted that Moore's initial condition

$$z(e, t=0) = e + \epsilon \sin e, \quad \gamma(e) = 1,$$

does not have this property as the cotangent in (3.4) induces all modes to contribute to $\partial z(e, t=0)/\partial t$.

The recursion relations for $Z_n(e)$ are derived by substituting (3.2) into (3.4) and equating like powers of time:

$$(n+1)\,Z^*_{n+1} + \sum_{j=0}^{n-1} (j+1)\,Z^*_{j+1} \frac{dZ_{n-j}}{de} = \frac{1}{4\pi i} \int_0^{2\pi} \sum_{j=0}^{n} R_j(e,e')\,V_{n-j}(e,e')\,de'. \tag{3.6}$$

Here

$$R_n = \gamma(e') \frac{dZ_n(e)}{de} - \gamma(e) \frac{dZ_n(e')}{de'}, \tag{3.7}$$

while V_n satisfies the recurrence relation

$$V_n(e,e') = -\tfrac{1}{2}[Z_n(e) - Z_n(e')] - \frac{1}{2n} \sum_{k=0}^{n-1} (k+1)\,(Z_{k+1}(e) - Z_{k+1}(e')) \sum_{j=0}^{n-k-1} V_j V_{n-j-k-1}, \tag{3.8}$$

with

$$Z_0(e) = e, \quad V_0(e) = \cot \tfrac{1}{2}(e - e'). \tag{3.9}$$

The functions $R_n(e,e')$ and $1/V_n(e,e')$ vanish linearly as $e \to e'$ so that the integrals in (3.6) are finite. To evaluate the required integrals it is convenient to define the quantities

$$\left.\begin{aligned} P_n(e,e') &= R_n(e,e')/(\cos e - \cos e'), \\ Y_n(e,e') &= (\cos e - \cos e')\,V_n(e,e'). \end{aligned}\right\} \tag{3.10}$$

Then, equations (3.6)–(3.8) become

$$Z^*_{n+1}(e) = \frac{1}{4\pi i (n+1)} \int_0^{2\pi} \sum_{j=0}^{n} P_j(e,e')\,Y_{n-j}(e,e')\,de' - \frac{1}{n+1} \sum_{j=0}^{n-1} (j+1)\,Z^*_{j+1} \frac{dZ_{n-j}}{de}, \tag{3.11}$$

$$P_n = \frac{\gamma(e')\,dZ_n(e)/de - \gamma(e)\,dZ_n(e')/de'}{\cos e - \cos e'}, \tag{3.12}$$

$$\begin{aligned} Y_n = &-\tfrac{1}{2}(Z_n(e) - Z_n(e'))\,(\cos e - \cos e') \\ &- \frac{1}{2n} \sum_{k=0}^{n-1} (k+1)\,(Z_{k+1}(e) - Z_{k+1}(e')) \sum_{j=0}^{n-k-1} \frac{Y_j Y_{n-j-k-1}}{\cos e - \cos e'}. \end{aligned} \tag{3.13}$$

We prove that $Z_n(e)$ is expansible as in (3.5) by induction. The result has already been shown for $n = 1$. Assume the result holds up to n. With the initial condition $\gamma(e) = 1 + a\cos e$ and noting the resulting odd symmetry of $z(e)$, it follows that the numerator in (3.12) is a difference of two polynomials in $\cos e$ and $\cos e'$. (Here we use the fact that $\cos ne$ is a polynomial in $\cos e$.) Such a function is always divisible by $\cos e - \cos e'$ so P_n has a finite Fourier series involving modes up to order n. Similar symmetry arguments may be applied to the recursion relation for Y_n to show that it has a finite Fourier series involving modes up to order $n+1$. Thus, $Z_{n+1}(e)$ may be expanded in terms of at most $n+1$ Fourier modes as in (3.5), completing the inductive proof.

The first 7 series coefficients have been computed exactly using the symbolic manipulation program MACSYMA (see the appendix). Contributions to the y co-ordinate of the interface occur for every odd order in t, while contributions to the x co-ordinate occur in every even order. It is easy to check that the Taylor series obtained for Fourier mode m including only its leading-order contribution, which is $O(a^m)$, is

the power series solution for $A_{m0}(t)$ (see § 2). At any order in time only a finite number of high-order corrections enter so it is possible to write the Taylor series for the subsystems A_{m2}, A_{m4}, and so on.

In order to gain further insight into the existence of the singularity it is necessary to carry the series computation much farther than the exact results given in the appendix to order t^7. This may be accomplished by performing the mounting algebraic work in floating-point arithmetic rather than symbolic arithmetic. An examination of the recurrence relations (3.11)–(3.13) shows that the computational time required to compute to order t^n is dominated by the nth derivative of the cotangent kernel, namely Y_n. As Y_n is a finite Fourier series in two variables with $O(n^2)$ terms, a straightforward calculation involving series multiplication and division requires $O(n^6)$ operations so the work necessary to obtain all coefficients of terms up to t^n grows like n^7 for large n.

It is possible to reduce the computational time to $O(n^5)$ by using transform methods (Orszag 1970). The Fourier series for Y_n may be written as a sum of separable functions:

$$Y_n(e,e') = \sum_{\substack{i,j \\ 0\leqslant i+j\leqslant n+1}}\sum D_{ij}[\sin(ie)\cos(je')+\sin(je)\cos(ie) + \sin(je)\cos(ie')+\sin(ie')\cos(je)]. \quad (3.14)$$

Using separability, the number of operations required to transform $Y_n(e,e')$ from its Fourier representation to configuration space at n discrete points in e and e' is $O(n^3)$ rather than $O(n^4)$. In configuration space only $O(n^4)$ operations are necessary to evaluate the right side of (3.13) so that the operation count to compute Y_n from $Y_k\,(k<n)$ and Z_n grows only like n^4. Once P_k, Y_k, and Z_k for $k<n$ have been evaluated in configuration space, $Z_{n+1}(e)$ is evaluated from (3.11) by computing the integrand and performing the integral. As the result must be a finite Fourier series in e, the integral may be evaluated exactly by the trapezoidal rule. A slight technical complication arises from the fact that it is inconvenient to evaluate P_k or Y_k at the points $e=e'$. While P_k and Y_k are certainly finite at these points, it is more efficient to apply an alternating Gaussian quadrature to perform the integral in (3.11) (see Menikoff & Zemach 1980). Finally, in order to proceed to higher n an inverse transform of P_n, Y_n, and Z_{n+1} is performed and their modal amplitudes are stored rather than their configuration space values. This allows more efficient use of memory resources as it becomes possible to take advantage of symmetries in the Fourier coefficients. Since the work involved at each step of this recursive procedure is $O(n^4)$, the total work necessary to calculate $Z_n(e)$ for $n\leqslant N$ is $O(N^5)$.

The coefficients $Z_n(e)$ have been computed for $n\leqslant 38$, when $a=1$ and $a=\frac{1}{16}$ and for $n\leqslant 24$ when $a=\frac{1}{2}, \frac{1}{4}$, and $\frac{1}{8}$. All calculations were performed with 96-bit mantissa arithmetic (29 digits of accuracy). The proper execution of the program has been checked for low orders using the exact results given in the appendix. At higher orders, a useful computational test is given by constructing the Taylor series for the energy of the system:

$$E=\int_0^{2\pi}\gamma(e')\,de'\int_0^{2\pi}\gamma(e)\,de\ln|\sin\tfrac{1}{2}(z(e,t)-z(e',t))|. \quad (3.15)$$

It can be shown using (1.3) that

$$\frac{dE}{dt}=0. \quad (3.16)$$

The Taylor series in t for $E(t)$ has a non-zero constant term while all higher-order terms vanish by virtue of (3.16). The nth time derivative of the energy is given by

$$E_{n+1} = \frac{1}{(n+1)} \int_0^{2\pi} \gamma(e')\, de' \int_0^{2\pi} \gamma(e)\, de \sum_{k=0}^{n} \frac{Y_k(e,e')}{\cos e - \cos e'} (k+1) \times \left(\frac{Z_{k+1}(e) - Z_{k+1}(e')}{2} \right) = 0 \quad (n \geqslant 0). \tag{3.17}$$

Equation (3.17) provides a non-trivial sum rule check on each stage of the computation and, with the proper scaling of the coefficients Z_n, gives an indication of the cumulative roundoff error incurred at each order. For the calculation to $O(t^{38})$ with $a = 1$ the computed coefficients are accurate to at least 12 significant digits.

4. Analysis of the Taylor series

A good way to examine $z(e,t)$ for possible singularities is to study its spectrum in e. For $t < t_c$, the spectrum seems to have the form

$$|A_m| \simeq Cm^{-\beta} \exp(-m\alpha(t)), \tag{4.1}$$

where $A_m(t)$ is defined by (1.5). Thus, the mean square gradients $\Omega^{(p)}$ of the interface defined by

$$\Omega^{(p)}(t) = \int_0^{2\pi} \left| \frac{\partial^p z}{\partial e^p} \right|^2 de = \sum_k k^{2p} |A_k|^2 = \sum_{n=0}^{\infty} \Omega_n^{(p)} t^{2n} \tag{4.2}$$

diverges at the critical time t_c defined by

$$\alpha(t_c) = 0, \tag{4.3}$$

provided

$$p \geqslant \tfrac{1}{2}(2\beta - 1). \tag{4.4}$$

Here the series expansion of $\Omega^{(p)}(t)$ involves only even powers of t because of time reversal invariance. Equation (4.3) is an effective way to determine the singularity time t_c, if it exists.

For $t \simeq t_c$, $\Omega^{(p)}(t)$ may be expected to behave like

$$\Omega^{(p)}(t) \simeq C_p (1 - t^2/t_c^2)^{-\delta(p)}, \tag{4.5}$$

so it will diverge or vanish according to the sign of the critical exponent $\delta(p)$. The function $\delta(p)$ gives an estimate for β in (4.1): If the spectrum of the interface at t_c behaved like $k^{-\beta}$ as $k \to \infty$ then the largest zero of $\delta(p)$ would be $p = \beta - \frac{1}{2}$.

The coefficients $\Omega_n^{(p)}$ for $p = 2, 3, 4, 5$ when $a = 1$ are listed in table 1. The analysis of these series borrows heavily from the methods devised by Domb & Sykes (Gaunt & Guttmann 1974), and Baker (1975) for expansions appearing in the study of critical phenomena.

From table 1 we see that the coefficients $\Omega_n^{(p)}$ are all of positive sign. This is an indication that the nearest singularity in the complex-t plane lies on the positive real axis. An examination of the ratios $\Omega_n^{(2)}/\Omega_{n-1}^{(2)}$ suggests that the region of convergence of the series (4.2) for $\Omega^{(2)}(t)$ is roughly $|t| < 1$. A more accurate estimation of the radius of convergence is obtained using a Domb–Sykes plot. In figure 3, the inverse ratios $\Omega_n^{(p)}/\Omega_{n-1}^{(p)}$ are plotted versus $1/n$. If the nearest singularity has the asymptotic form

$$\left.\begin{aligned} &\Omega \simeq C(t_c - t)^{-\delta} \quad (\delta \neq 0, 1, 2, \ldots) \\ \text{or} \quad &\Omega \simeq C(t_c - t)^{-\delta} \ln(t_c - t) \quad (\delta = 0, 1, 2, \ldots), \end{aligned}\right\} \tag{4.6}$$

n	$\Omega^{(2)}$	$\Omega^{(3)}$	$\Omega^{(4)}$	$\Omega^{(5)}$
0	0	0	0	0
1	0·125 000 000	0·125 000 000	0·125 000 000	0·125 000 000
2	$0{\cdot}390\,625\,000 \times 10^{-01}$	0·132 812 500	0·507 812 500	$0{\cdot}200\,781\,250 \times 10^{01}$
3	$0{\cdot}923\,394\,097 \times 10^{-02}$	$0{\cdot}391\,818\,576 \times 10^{-01}$	0·158 973 524	0·638 140 191
4	$0{\cdot}504\,416\,814 \times 10^{-02}$	$0{\cdot}429\,388\,621 \times 10^{-01}$	0·416 990 783	$0{\cdot}453\,069\,114 \times 10^{01}$
5	$0{\cdot}271\,300\,166 \times 10^{-02}$	$0{\cdot}321\,708\,860 \times 10^{-01}$	0·420 877 972	$0{\cdot}593\,048\,079 \times 10^{01}$
6	$0{\cdot}174\,238\,933 \times 10^{-02}$	$0{\cdot}288\,336\,815 \times 10^{-01}$	0·533 978 858	$0{\cdot}108\,533\,594 \times 10^{02}$
7	$0{\cdot}115\,871\,681 \times 10^{-02}$	$0{\cdot}249\,430\,831 \times 10^{-01}$	0·597 037 690	$0{\cdot}155\,040\,962 \times 10^{02}$
8	$0{\cdot}812\,562\,331 \times 10^{-03}$	$0{\cdot}220\,992\,160 \times 10^{-01}$	0·668 313 975	$0{\cdot}219\,459\,403 \times 10^{02}$
9	$0{\cdot}584\,792\,497 \times 10^{-03}$	$0{\cdot}195\,277\,639 \times 10^{-01}$	0·723 338 279	$0{\cdot}290\,074\,910 \times 10^{02}$
10	$0{\cdot}431\,048\,874 \times 10^{-03}$	$0{\cdot}173\,085\,649 \times 10^{-01}$	0·769 785 458	$0{\cdot}370\,182\,782 \times 10^{02}$
11	$0{\cdot}323\,085\,485 \times 10^{-03}$	$0{\cdot}153\,331\,115 \times 10^{-01}$	0·804 555 413	$0{\cdot}455\,777\,991 \times 10^{02}$
12	$0{\cdot}245\,582\,826 \times 10^{-03}$	$0{\cdot}135\,808\,124 \times 10^{-01}$	0·829 064 252	$0{\cdot}545\,741\,516 \times 10^{02}$
13	$0{\cdot}188\,769\,587 \times 10^{-03}$	$0{\cdot}120\,196\,732 \times 10^{-01}$	0·843 582 801	$0{\cdot}637\,658\,979 \times 10^{02}$
14	$0{\cdot}146\,468\,791 \times 10^{-03}$	$0{\cdot}106\,296\,617 \times 10^{-01}$	0·849 078 269	$0{\cdot}729\,686\,076 \times 10^{02}$
15	$0{\cdot}114\,547\,342 \times 10^{-03}$	$0{\cdot}939\,210\,294 \times 10^{-02}$	0·846 452 226	$0{\cdot}819\,907\,315 \times 10^{02}$
16	$0{\cdot}901\,909\,211 \times 10^{-04}$	$0{\cdot}829\,127\,558 \times 10^{-02}$	0·836 717 451	$0{\cdot}906\,668\,172 \times 10^{02}$
17	$0{\cdot}714\,297\,727 \times 10^{-04}$	$0{\cdot}731\,300\,987 \times 10^{-02}$	0·820 871 036	$0{\cdot}988\,501\,060 \times 10^{02}$
18	$0{\cdot}568\,609\,095 \times 10^{-04}$	$0{\cdot}644\,462\,382 \times 10^{-02}$	0·799 890 201	$0{\cdot}106\,418\,611 \times 10^{03}$
19	$0{\cdot}454\,675\,424 \times 10^{-04}$	$0{\cdot}567\,463\,898 \times 10^{-02}$	0·774 699 672	$0{\cdot}113\,274\,246 \times 10^{03}$

TABLE 1. Coefficients $\Omega_n^{(p)}$ $(0 \leqslant n \leqslant 19)$ of the series expansion of $\Omega^{(p)}(t)$ in powers of t^2 when $a = 1$

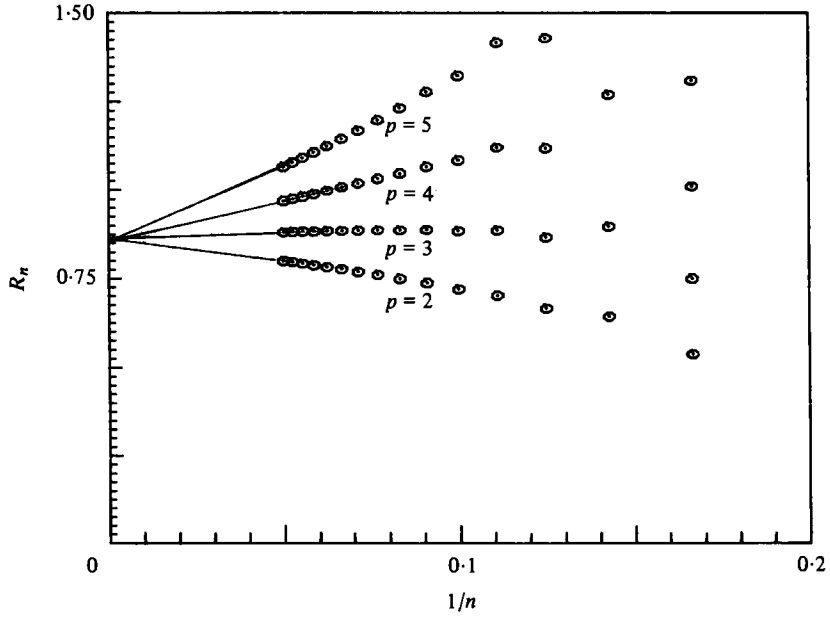

FIGURE 3. A Domb–Sykes plot of the ratios $R_n = \Omega_n^{(p)}/\Omega_{n-1}^{(p)}$ versus $1/n$ for $p = 2, 3, 4, 5$ for the initial condition (1.8) with $a = 1$. The straight line extrapolations correspond to Neville table estimates for $1/t_c^2$. Note that all four series seem to have a singularity at $t_c \simeq 1{\cdot}08$.

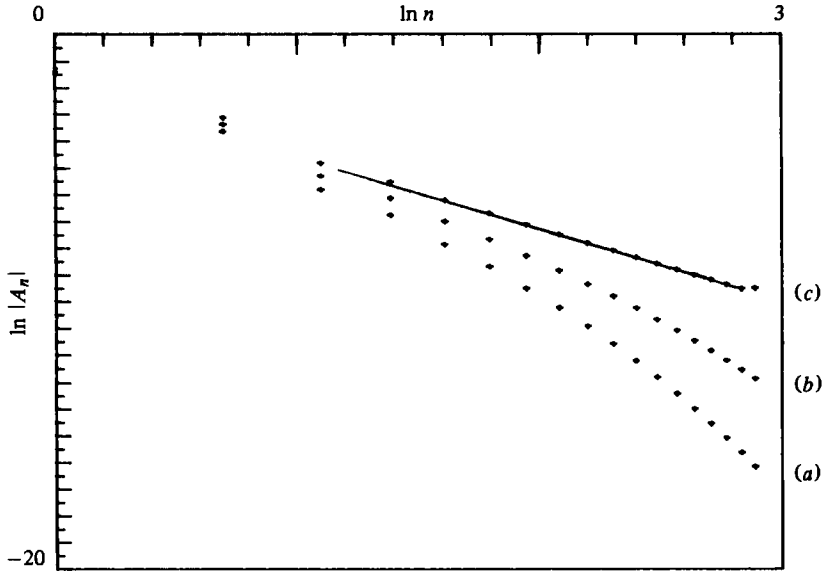

FIGURE 4. A plot of $\ln|A_n|$ *vs.* $\ln n$ for the initial condition (1.8) with $a = 1$ at times (*a*) $t = 0{\cdot}864$, (*b*) $t = 0{\cdot}972$, (*c*) $t = 1{\cdot}08$. The straight line fit gives a slope of $\beta \simeq 2{\cdot}7$.

then from Darboux's theorem the inverse ratios $R_n^{(p)} = \Omega_n^{(p)}/\Omega_{n-1}^{(p)}$ behave like $1/n$ as $n \to \infty$ with

$$R_n^{(p)} \simeq \frac{1}{t_c^2}\left[1 - \frac{1-\delta}{n} + O(1/n^2)\right], \tag{4.7}$$

Examination of the Domb–Sykes plots for $\Omega^{(p)}$ reveals that all four functions may have a common singularity. Estimates based on the Neville table and Padé approximants suggest that the critical time for $a = 1$ is

$$t_c = 1{\cdot}08 \pm 0{\cdot}02.$$

If the mode amplitudes A_n behave like $n^{-\frac{1}{2}}$ $(n \to \infty)$ at t_c then the critical exponent $\delta(2)$ for $\Omega^{(2)}(t)$ should be close to 0. Examination of the Domb–Sykes plot shows that $\delta(2) \simeq -0{\cdot}5 \pm 0{\cdot}1$. A crude linear interpolation of $\delta(p)$ *vs.* p indicates that the largest zero of $\delta(p)$ occurs for $p \simeq 2{\cdot}3$, which implies that A_n behaves like $n^{-\beta}$ as $n \to \infty$ with $\beta \simeq 2{\cdot}8$ rather than $\beta = 2{\cdot}5$. A more direct estimate of β is obtained by plotting $\ln|A_n(t)|$ versus $\ln n$ near the singularity time as was done in the previous section for the subsystem A_{n0}. The values of $A_n(t)$ were computed by Padé summation of the time series for each mode. The number of series terms computed for $A_n(t)$ decreases with increasing n so that reliable Padé estimates are available near the singularity time only for the first 15 modes. The results plotted in figure 4 are consistent with a value of $\beta = 2{\cdot}7 \pm 0{\cdot}2$.

We have performed identical series analyses on $\Omega^{(p)}(t)$ for $a = \frac{1}{2}$, $\frac{1}{4}$, $\frac{1}{8}$ and $\frac{1}{16}$ in order to examine the variation of t_c with a. These series have been computed to $O(t^{24})$ ($O(t^{38})$ for $a = \frac{1}{16}$). Again the coefficients are all of positive sign indicating that the nearest singularities lie on the real time axis. The best estimates from Domb–Sykes plots and Padé tables for $t_c(a)$ are plotted in figure 5. For purposes of comparison the prediction (2.9) of Moore's asymptotic analysis is also plotted. It is clear that, as

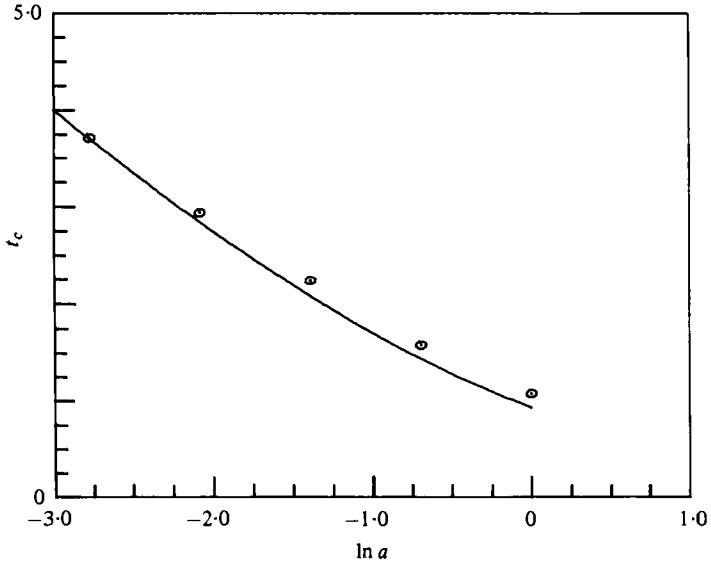

FIGURE 5. A plot of t_c *vs.* ln a for the initial condition (1.8). The solid line is Moore's leading-order asymptotic approximation to $t_c(a)$ given by (2.8).

$a \to 0$, the critical times agree qualitatively with the asymptotic result (2.9). For $a = O(1)$, the critical time is underestimated by (2.9).

Using the series analysis methods, it is difficult to obtain reliable estimates for t_c for values of a less than $\frac{1}{16}$. The distance between the putative singularity and the origin ($t = 0$) increases as $a \to 0$ and so more coefficients in the series are necessary in order to resolve the analytic background and the singularity.

It is of interest to use the high-order Taylor series in t for the modes in order to simulate the evolution of the sheet. Since $A_n \simeq n^{-2.7}$ at $t = t_c$ the interface itself remains smooth as does its first derivative with respect to position. The curvature diverges weakly along some portion of the interface, as do all higher derivatives.

We have used Padé approximants in t to evaluate the Fourier coefficient $A_n(t)$ in (1.5). We also apply Padé approximants in e for fixed t to estimate the sum of (1.5). In figures 6 and 7, the interface $x(e) + iy(e)$ and the true vortex sheet strength

$$\omega = \gamma(e)/((dx/de)^2 + (dy/de)^2)^{\frac{1}{2}},$$

respectively, are plotted as functions of x. As the sheet compresses about the point of roll-up the sheet strength ω increases. At the singularity time the vorticity distribution forms a cusp. When the singularity first forms, the interface is only slightly distorted and possesses none of the features associated with sheet roll-up (as previously noted by Moore).

5. Conclusions

The use of extended time series in analysing our prototype of Kelvin–Helmholtz instability is by no means a rigorous procedure. The indications that a physical singularity can form in a finite time are only suggestive, and deeper analysis is required to justify rigorously the existence of such a singularity. Coupled with the work of Moore

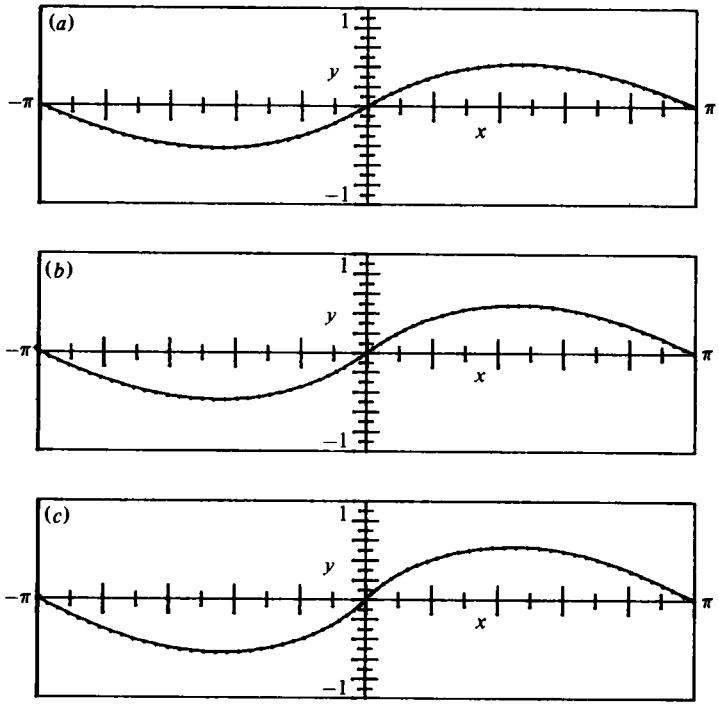

FIGURE 6. A plot of the interface $z(\epsilon, t)$ for the initial condition (1.8) with $a = 1$ at times (*a*) $t = 0{\cdot}864$, (*b*) $t = 0{\cdot}972$, and (*c*) $t = 1{\cdot}08$. Note that at the singularity time $t_c \simeq 1{\cdot}08$ the interface is only slightly deformed.

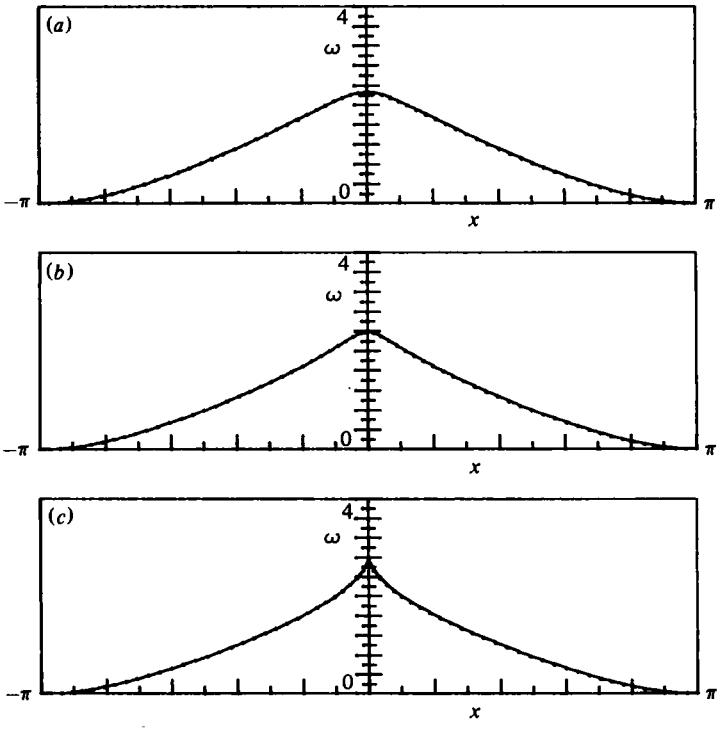

FIGURE 7. A plot of the vortex sheet strength $\omega(x, t)$ *vs.* x (see text) for the initial condition (1.8) with $a = 1$ at times (*a*) $t = 0{\cdot}864$, (*b*) $t = 0{\cdot}972$ and (*c*) $t = 1{\cdot}08$. Note that at the singularity time $\omega(x, t)$ has a cusp at the roll-up point $x = 0$.

(1979) and Damms (unpublished), our results do provide evidence that the vortex sheet model is valid for only a finite time unless the sheet undergoes sufficiently rapid stretching (Moore 1976; Moore & Griffith-Jones 1974).

The slight differences between the observed algebraic behaviour at $t = t_c$ for the amplitudes $|A_n|$ and the asymptotic estimates may be attributable to the moderate values of a used in this work. Moore's asymptotic theory is only valid when $-\ln a \gg 1$. However, for $a = \frac{1}{16}$ the measured spectrum is still roughly $n^{-2\cdot7}$, although the uncertainty is greater here as fewer reliable modes are available. The higher-amplitude corrections $A_{n2}, A_{n4}, \ldots$ may be appreciable for the present range of values of a, but it is also possible that for our prototype these corrections behave in a different way from the case analysed by Moore. Finally, it is known that the self-consistent measures of accuracy in series analysis methods can be misleading (Nickel 1980) and so we have assigned what we felt to be conservative error bars in assessing the data.

One extension of the present work is to the study of the analytic structure of two-layer irrotational dynamics where buoyancy, surface tension, and pressure forces are taken into account. For these cases, the function $\gamma(e)$ is no longer a Lagrangian invariant. If only buoyancy effects are considered $\gamma(e,t)$ satisfies the equation (Baker, Meiron & Orszag 1980)

$$\frac{\partial \gamma(e,t)}{\partial t} = 2\left(\frac{\rho'-\rho}{\rho'+\rho}\right)\left[g\mathscr{I}\left(\frac{\partial z}{\partial e}\right)+\frac{1}{8}\frac{\partial}{\partial e}\left(\frac{\gamma^2}{\left(\frac{\partial x}{\partial e}\right)^2+\left(\frac{\partial y}{\partial e}\right)^2}\right)+\mathscr{R}\left(\frac{\partial^2 z^*}{\partial t^2}\frac{\partial z}{\partial e}\right)\right]. \tag{5.1}$$

Baker *et al.* (1980) have used (5.1) together with (1.3) to simulate the Rayleigh–Taylor instability numerically. For the values of the Atwood ratio

$$0 < (\rho'-\rho)/(\rho'+\rho) < 1,$$

the interface rolls up due to Helmholtz instability and the vortex sheet model becomes unreliable. For Atwood ratio 1 in which the fluid falls freely into a vacuum there is no roll-up and an increase in the number of retained vortices does improve the description of the sheet.

It can be shown that, for an initial condition of the form

$$\gamma(e, t=0) = a\sin e, \quad z(e, t=0) = e, \tag{5.2}$$

the interface and $\gamma(e,t)$ have Taylor series of the form

$$\left.\begin{aligned} x(e,t) &= e + \sum_{n=1}^{\infty} t^n \sum_{j=0}^{n} X_{nj}\sin je, \\ y(e,t) &= \sum_{n=1}^{\infty} t^n \sum_{j=0}^{n} Y_{nj}\cos je, \\ \gamma(e,t) &= \sum_{n=0}^{\infty} t^n \sum_{n=0}^{n+1} \Gamma_{nj}\sin je. \end{aligned}\right\} \tag{5.3}$$

so that these systems may be studied for any Atwood ratio by the methods discussed above. Results for these prototype problems will be presented in a later paper.

Similarly, prototypical free-surface wave-dynamical problems may be constructed. Baker, Meiron & Orszag (1982) have successfully applied vortex techniques to a wide variety of nonlinear surface and internal wave phenomena. The mathematical structure of prototype problems may be studied by the present techniques.

We would like to thank B. G. Nickel, R. L. McCrory, U. Frisch, R. H. Morf and C. P. Verdon for helpful discussions. This work was supported by the Office of Naval Research under contracts no. N00014-77-C-0138 and N00014-79-C-0478, the Los Alamos Scientific Laboratory which is supported by the U.S. Department of Energy and the National Science Foundation under Grant ATM-8017284.

Appendix

The Taylor-series coefficients $Z_n(e)$ for $0 \leqslant n \leqslant 7$ of the interface $z(e,t)$ for the initial condition (1.8):

$$Z_0(e) = e;$$

$$Z_1(e) = \tfrac{1}{2}i[a\sin e];$$

$$Z_2(e) = \tfrac{1}{4}[-\tfrac{1}{2}a\sin e - \tfrac{1}{4}a^2\sin 2e];$$

$$Z_3(e) = \tfrac{1}{8}i[\tfrac{1}{8}(a-a^3)\sin e + \tfrac{1}{12}a^2\sin 2e];$$

$$Z_4(e) = \tfrac{1}{16}[(-\tfrac{1}{24}a - \tfrac{1}{48}a^3)\sin e + (-\tfrac{3}{16}a^2 + \tfrac{1}{24}a^4)\sin 2e - \tfrac{7}{48}a^3\sin 3e - \tfrac{1}{32}a^4\sin 4e];$$

$$\begin{aligned} Z_5(e) = {} & \tfrac{1}{32}i[(\tfrac{1}{120}a - \tfrac{7}{48}a^3 + \tfrac{7}{120}a^5)\sin e + (\tfrac{17}{240}a^2 - \tfrac{1}{8}a^4)\sin 2e \\ & + (\tfrac{1}{16}a^3 - \tfrac{1}{48}a^5)\sin 3e + \tfrac{7}{480}a^4\sin 4e]; \end{aligned}$$

$$\begin{aligned} Z_6(e) = {} & \tfrac{1}{64}[(-\tfrac{1}{720}a - \tfrac{1}{16}a^3 + \tfrac{17}{480}a^5)\sin e + (-\tfrac{13}{288}a^2 + \tfrac{1}{144}a^4 - \tfrac{11}{720}a^6)\sin 2e \\ & + (-\tfrac{37}{240}a^3 + \tfrac{41}{900}a^5)\sin 3e + (-\tfrac{13}{80}a^4 + \tfrac{17}{1440}a^6)\sin 4e \\ & - \tfrac{199}{2880}a^5\sin 5e - \tfrac{1}{96}a^6\sin 6e]; \end{aligned}$$

$$\begin{aligned} Z_7(e) = {} & \tfrac{1}{128}i[(\tfrac{1}{5040}a - \tfrac{61}{2520}a^3 + \tfrac{167}{5040}a^5 - \tfrac{9}{280}a^7)\sin e \\ & + (\tfrac{43}{3360}a^2 - \tfrac{1457}{10080}a^4 + \tfrac{151}{2240}a^6)\sin 2e + (\tfrac{101}{1680}a^3 - \tfrac{949}{6720}a^5 + \tfrac{13}{840}a^7)\sin 3e \\ & + (\tfrac{361}{5040}a^4 - \tfrac{95}{2016}a^6)\sin 4e + (\tfrac{221}{6720}a^5 - \tfrac{1}{210}a^7)\sin 5e + (\tfrac{53}{10080}a^6)\sin 6e]. \end{aligned}$$

REFERENCES

BAKER, G. A. 1975 *Essentials of Padé Approximants*. Academic.

BAKER, G. R., MEIRON, D. I. & ORSZAG, S. A. 1980 Vortex simulations of the Rayleigh–Taylor instability. *Phys. Fluids* **23**, 1485.

BAKER, G. R., MEIRON, D. I. & ORSZAG, S. A. 1982 Generalized vortex methods for free surface flow problems. (To appear.)

BIRKHOFF, G. 1962 Helmholtz and Taylor instability in hydrodynamic instability. *Proc. Symp. on Applied Math.* XIII. A.M.S.

GAUNT, D. S. & GUTTMANN, A. J. 1974 Asymptotic analysis of coefficients. In *Phase Transitions and Critical Phenomena*, vol. 3. Academic.

MENIKOFF, R. & ZEMACH, C. 1980 Methods for numerical conformal mapping. *J. Comp. Phys.* **36**, 366.

MOORE, D. W. 1976 The stability of an evolving two-dimensional vortex sheet. *Mathematika* **23**, 35.

MOORE, D. W. 1979 The spontaneous appearance of a singularity in the shape of an evolving vortex sheet. *Proc. R. Soc. Lond.* A **365**, 105.

MOORE, D. W. & GRIFFITH-JONES, R. 1974 The stability of an expanding circular vortex sheet. *Mathematika* **21**, 128.

MORF, R. H., ORSZAG, S. A. & FRISCH, U. 1980 Spontaneous singularity in three-dimensional, inviscid, incompressible flow. *Phys. Rev. Lett.* **44**, 572.

NICKEL, B. G. 1980 In *Cargèse Lectures in Physics*. Plenum.

Orszag, S. A. 1970 Transform method for the evaluation of vector-coupled sums: Application to the spectral form of the vorticity equation. *J. Atmos. Sci.* **27**, 890.

Saffman, P. G. & Baker, G. R. 1979 Vortex interactions. *Ann. Rev. Fluid Mech.* **11**, 95.

Sulem, C., Sulem, P. L., Bardos, C. & Frisch, U. 1982 Finite time analyticity for the two and three dimensional Kelvin–Helmholtz instability. (To appear.)

Van de Vooren, A. T. 1965 A numerical investigation of the rollup of vortex sheets. *Dept. Math. Groningen Univ., The Netherlands, Rep.* TW-21.